Plasmon Enhanced Two-Photon Probing with Gold and Silver Nanovoid Structures

*Fani Madzharova, Denis Öhl, João Junqueira, Wolfgang Schuhmann,
and Janina Kneipp**

Nonlinear optical signals benefit greatly from the enhanced local optical fields in the vicinity of plasmonic nanostructures. Gold and silver nanovoid arrays of varying size and thickness, fabricated by electrochemical deposition are shown here to act as stable plasmonic nanostructures and to enhance the weak, incoherent two-photon excited process of surface-enhanced hyper Raman scattering (SEHRS) with high microscopic homogeneity and reproducibility that typical SEHRS experiments have not been addressing so far. Silver nanovoids yield stronger enhancement than gold voids, but gold nanovoid arrays show improved stability at high laser excitation intensities. Combined screening experiments using SEHRS and second-harmonic generation (SHG) reveal a dependence of the enhancement of both signals on void structural parameters and similar optimum geometries for both two-photon processes. The results confirm the suggested important role for the enhancement of the near-infrared excitation field in SEHRS and suggest SHG as a fast screening tool to identify nanostructures that can support high SEHRS enhancement.

1. Introduction

Two-photon spectroscopy and microscopy have gained increasing importance in probing of light–matter interaction because of the many advantages that come with the use of light in the near infrared wavelength range. This includes for example the high confinement of focal volumes and contributions of higher-order terms in the induced dipole moment, providing valuable information on molecular structure and symmetry.[1] Since they rely on the simultaneous action of two

F. Madzharova, Prof. J. Kneipp
Department of Chemistry
Humboldt-Universität zu Berlin
Brook-Taylor-Str. 2, 12489 Berlin, Germany
E-mail: janina.kneipp@chemie.hu-berlin.de
D. Öhl, J. Junqueira, Prof. W. Schuhmann
Analytical Chemistry – Center for Electrochemical Sciences (CES)
Faculty of Chemistry and Biochemistry
Ruhr University Bochum
Universitätsstraße 150, 44780 Bochum, Germany

The ORCID identification number(s) for the author(s) of this article can be found under https://doi.org/10.1002/adom.201900650.

photons, incoherent nonlinear processes such as two-photon fluorescence or hyper Raman scattering (HRS)[2] are very weak. Nonresonant HRS, with extremely small cross sections on the order of 10^{-65} cm^4 s photon^{-1}, does not constitute a useful spectroscopic tool, unless molecular resonance is exploited.[3] Nevertheless, since nonlinear, two-photon processes depend on the square of the excitation photon flux density, they benefit extremely from an enhancement by high local optical fields.[4] Thereby, they gain practical importance: Surface enhanced hyper Raman scattering (SEHRS),[5] the spontaneous two-photon excited Raman process occurring in the highly confined electromagnetic fields of plasmonic nanostructures[4c] is a complementary approach to (one-photon excited) surface enhanced Raman scattering (SERS).[6] It provides additional vibrational information due to the different selection rules acting in Raman and HRS.[7] In particular, SEHRS is more sensitive than SERS with respect to molecular orientation and surface environmental changes.[8] Therefore, SEHRS is often used in combination with SERS for the structure elucidation of organic and bioorganic molecules,[8d,9] microenvironmental sensing,[8b,10] and spectroscopic imaging.[11]

Obtaining comprehensive vibrational and imaging information by means of SEHRS requires plasmonic nanostructures that provide homogeneous and strong plasmonic enhancement. The morphology of roughened electrodes used in early SEHRS experiments[8a,12] and of typical nanoparticle substrates for SEHRS[8e,13] is controllable only to a limited extent, and the enhancement by nanoparticles is strongly influenced by the presence and interaction of analyte molecules.[13] Well-defined, top-down fabricated plasmonic structures with nanoscale gaps that are used in SERS[14] could be also beneficial for SEHRS experiments.[15] Nevertheless, apart from the requirements of fabrication by lithography, recent theoretical and experimental work[9c,10c,16] indicates that an independent design and optimization of SEHRS substrates would be useful, due to the nonlinear dependence of SEHRS on the excitation field $|E(\nu_L)|^4|E(2\nu_L - \nu_{HRS})|^2$ and the wide spectral separation of excitation and scattered light.

During excitation of incoherent HRS or two-photon fluorescence, also other nonlinear, coherent optical signals can be obtained from a sample. Second-harmonic generation (SHG) is a two-photon process, where a non-centrosymmetric macromolecule or nanostructure yields an effective combination of
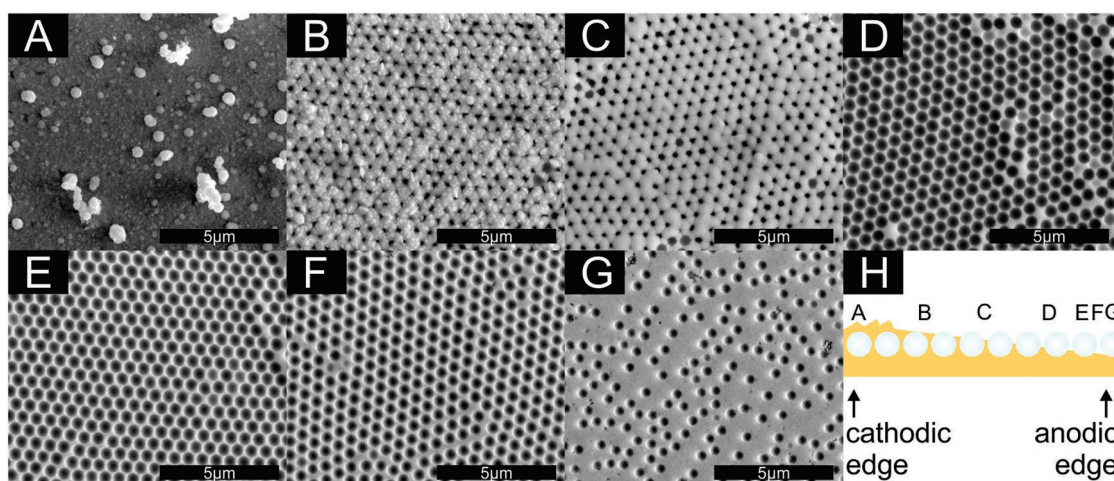
Figure 1. A–G) Scanning electron micrographs of an Au(600) gradient sample starting from the cathodic edge (A) and increasing distance from it (B–G). The distances from the cathodic edge in (B–G) are as follows: 5 mm (B), 8.5 mm (C), 17.5 mm (D), 19 mm (E), 20 mm (F), and 21 mm (G). H) Schematic representation of the metal thickness gradient across the bipolar electrode. The letters A–G represent approximately the positions from which the SEM images in (A–G) were taken.

two photons into a single photon of twice the frequency of the incident beam. The local fields of plasmonic nanostructures can also enhance the second harmonic radiation.[17]

In this work, we have fabricated nanostructured gold and silver films by electrodeposition comprised of periodically arranged spherical voids. We show that these nanovoid structures are specifically suitable for the enhancement of HRS and SHG at near IR excitation. Nanovoid arrays were shown to support a variety of plasmon modes in the visible and near IR, depending on their structural parameters[18] and are suitable for enhancement in SERS.[19] Reproducible void films with various geometries can be obtained by different fabrication methods, including electrochemical deposition,[19a] which is inexpensive and rapid compared to nanolithographic approaches.[19d,20] Here, gold and silver nanovoids with a thickness gradient and differently sized nanosphere templates are fabricated using bipolar electrodeposition.[21] Void structural parameters that result in the strongest two-photon signals were identified based on microspectroscopic experiments, and films of nanovoids with uniform thickness according to the optimized geometries were fabricated in a very reproducible fashion yielding tunable and stable plasmonic substrates for SEHRS and SHG studies. As will be discussed, the data confirm the important role of the near-IR excitation field in SEHRS enhancement. Furthermore, they indicate that the correlation between both two-photon excited processes enables us to use SHG as a fast screening tool for localization of those nanostructures providing high SEHRS enhancement, thereby opening a new perspective for utilizing SEHRS as efficient spectroanalytical approach.

2. Results and Discussion

To prepare the nanovoid structures, evaporated gold and silver thin films on a silicon wafer were patterned with a monolayer of polystyrene nanospheres with diameters of 200, 300, and 600 nm, respectively, using the Langmuir–Blodgett technique.

Then, a metal layer with a thickness gradient along the length of the sample was generated by means of bipolar electrochemistry (see Supporting Information for more details and Figure S1 in the Supporting Information for schematic of the bipolar electrodeposition).[21] After subsequent dissolution of the template beads, the resulting sample surfaces consist of a metal film comprised of periodically arranged voids that gradually change their opening sizes and interhole distances according to the metal film thickness. As examples of how the void structure changes at different positions along the length of the sample, **Figure 1** presents scanning electron micrographs of gold voids templated with 600 nm diameter nanospheres. Close to the cathodic pole, the gold deposition rate is highest leading to a very thick gold layer with the template polystyrene beads overgrown with an amorphous metal layer (Figure 1A). With increasing distance from the cathodic edge of the bipolar electrode (BE), the voids start to appear, and their opening sizes increase until the metal film reaches the equator of the template spheres (Figure 1B–D). From this point, the void diameter starts to decrease and a gold film with shallow structures and larger distances between the voids are formed (Figure 1E–G). The distance from the cathodic edge of the BE as a measure for the metal film thickness depends on variation in the BE length and hence on the variation of the potential gradient during deposition.

We investigated the nonlinear optical properties of the gradient void substrates by using femtosecond excitation at 850 nm and recording the backscattered SHG. **Figure 2**A shows the intensity of the SHG signal from a gold nanovoid gradient sample with a 200 nm nanosphere template, termed Au(200) gradient here, at different positions along the thickness gradient. SHG signals are observed at the cathodic edge of the BE (Figure 2A, from 1 to 5 mm), where the spheres are overgrown with a rough gold layer. In agreement with previous reports, the overgrowing metal film can provide a nanoscopic roughness that can lead to strong enhancement of second harmonic signals in localized hot spots.[22] The SHG signals become
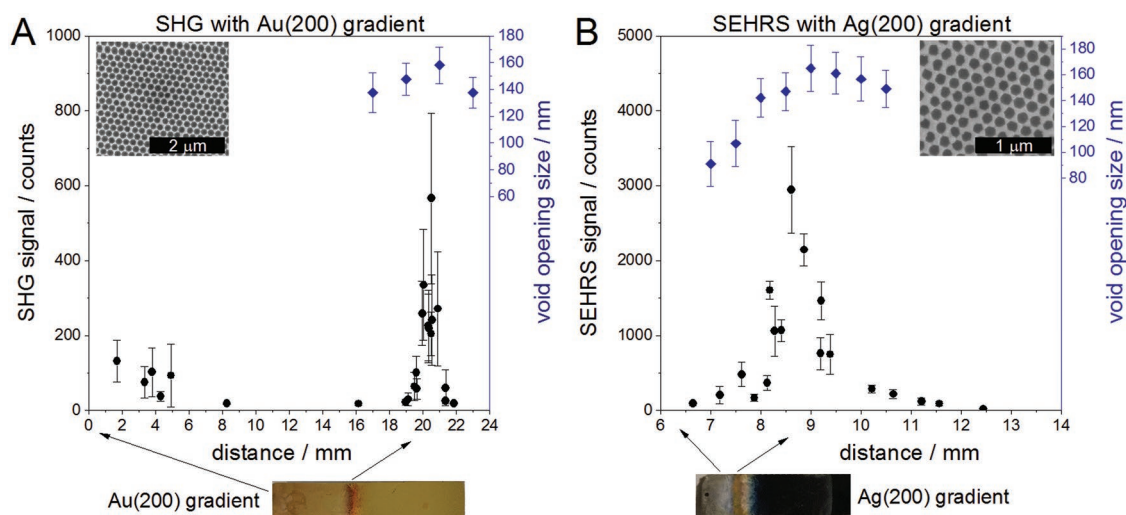
**ADVANCED
SCIENCE NEWS**
www.advancedsciencenews.com

**ADVANCED
OPTICAL
MATERIALS**
www.advopticalmat.de

Figure 2. A) SHG signal at 425 nm from an Au(200) nanovoid gradient sample, and B) SEHRS signal of the crystal violet band at 1585 cm^{-1} obtained with an Ag(200) nanovoid gradient as a function of the distance from the cathodic edge of the substrate. The data points represent the average value of the respective signal obtained after raster scanning areas of ≈100 µm × 100 µm of the sample with a step size of 10–30 µm (corresponding to averages over 100 values for SHG and 10 spectra for SEHRS). Excitation: 850 nm (A) and 1064 nm (B); acquisition time: 1 s (A) and 60 s (B), laser peak intensity: 7×10^9 Wcm^{-2} (A) and 1×10^{10} Wcm^{-2} (B). The right blue y-axes show the void opening sizes at the respective distances, as determined from SEM. Photographs of the samples are shown below the x-axes, and the arrows indicate the approximate positions relative to the cathodic edge. The insets show SEM images of the nanovoid substrates at the positions where the highest signals were observed (at 20.6 mm for the SHG signal maximum in (A), and at 8.6 mm for the SEHRS maximum in (B)).

weaker with increasing distance from the cathodic edge, when the gold deposition rate is diminished and the surface roughness slightly decreases (Figure 2A, from 6 to 15 mm). In the sample shown in Figure 2A, defined nanovoids above the equatorial plane without an overgrowing gold layer start appearing at a distance of 16 mm, void opening sizes are indicated on the right axis. From there, with further increasing distance, the SHG intensity increases until it reaches a maximum where nanovoid structures with an opening size of 150 nm above the equatorial plane are present (Figure 2A, from 18 to 20.6 mm). Further decreasing of the gold layer thickness results in very rapid decrease of the SHG intensity (Figure 2A, from 21 to 22 mm). The gold and silver samples obtained with 300 and 600 nm nanosphere templates display a similar variation of the SHG signals across the length of their respective BEs (data not shown). According to previous discussions, electromagnetic fields in nanovoid arrays can be significantly enhanced[19b,e,23] because of resonances with different, coexisting plasmon modes in the visible and/or near infrared, which can be tuned by altering the void diameter and height.[18a,b,24] Therefore, we infer that the observed SHG in these void structures must be plasmon enhanced as the result of resonances of the array modes with the excitation and/or second harmonic radiation wavelengths. The increasing and decreasing SHG intensity along the thickness gradient implies that the enhancement of SHG at the given excitation wavelength of 850 nm is different for the different void heights that are present along the sample length. This is in accordance with previous reports of a variation of electromagnetic enhancement in SERS excitation profiles with nanovoid structures.[19c,25]

The gradient nanovoid samples were evaluated for enhancement of two-photon vibrational spectra in HRS using crystal violet as test molecule. Crystal violet solution (10^{-5} M) was

placed on top of the nanovoid substrates, and SEHRS spectra were collected using picosecond laser excitation at 1064 nm. Alike the SHG signal, also the SEHRS enhancement varies along the length of the substrates, with gradual changes with the height of the voids. Figure 2B shows the SEHRS signal of the crystal violet vibration at 1585 cm^{-1} for a silver void gradient sample made with 200 nm sphere templates, termed Ag(200). The SEHRS intensity increases with increasing size of the void opening from 80 to 140 nm (Figure 2B, from 6.5 to 8.5 mm). The SEHRS signal reaches a maximum for voids with 147 nm diameter and height above the equatorial plane of the spheres. The SEHRS intensity decreases again with decreasing void opening size, and the last spectra were obtained with Ag(200) from voids with a diameter of 130 nm and a silver thickness below the equator of the template spheres at 11.5 mm distance from the cathodic edge of the BE (Figure 2B).

We observed SEHRS and SHG from both gold and silver gradient void structures fabricated with 200, 300, and 600 nm nanosphere templates. The void diameters from all substrates yielding the maximum SHG and SEHRS signals were determined from scanning electron microscopy (SEM) images taken at the respective positions of the samples (**Table 1**). Figure S2 in the Supporting Information shows the histograms of the void size distributions at those positions. Table 1 shows that most nanovoid sizes that yielded strongest 1064 nm-excited SEHRS agree (within the precision of the diameter measurements) with the sizes that result in maximum SHG signals at 850 nm excitation (compare second and fourth row in Table 1). Comparing the sizes of silver nanovoids that give the highest enhancement in SEHRS with those that have been reported in previous work[21a] to result in the highest one-photon SERS signals employing the same template spheres we find that optimum void structures for 1064 nm excited SEHRS and 532 nm excited

**ADVANCED
SCIENCE NEWS**

www.advancedsciencenews.com

**ADVANCED
OPTICAL
MATERIALS**

www.advopticalmat.de

Table 1. Void opening sizes that yielded the highest SHG (at 850 nm) and SEHRS (at 1064 nm) signals along the gold and silver gradient samples with 200, 300, and 600 nm nanosphere templates as determined from SEM. Below the respective row the normalized thickness $\bar{t}$ for each structure was calculated from the void diameter using the relations depicted in Figure S6 in the Supporting Information.

Void gradient	Ag(200)	Au(200)	Ag(300)	Au(300)	Ag(600)	Au(600)
SHG	141 ± 6 nm	150 ± 7 nm	238 ± 6 nm	248 ± 13 nm	356 ± 13 nm	470 ± 20 nm
$\bar{t}$	0.85	0.83	0.80	0.78	0.90	0.81
SEHRS	147 ± 10 nm	156 ± 16 nm	222 ± 16 nm	231 ± 11 nm	401 ± 19 nm	447 ± 45 nm
$\bar{t}$	0.84	0.81	0.84	0.82	0.87	0.83

SERS are very different. This provides further evidence that the plasmonic enhancement of the near-IR excitation field plays a more important role in the electromagnetic enhancement of SEHRS than the visible hyper Raman field, in agreement with a recent discussion on the enhancement of SEHRS with plasmonic nanoparticles in solution and on surfaces.[13] For void arrays obtained with 200 and 300 nm sphere templates, respectively, the void opening sizes yielding the highest signals in both SEHRS and SHG are almost the same for gold and silver (Table 1). Interestingly, the calculated normalized thickness from the determined void diameters (Table 1), assuming ideal geometries, is ≈0.8 for all structures, independent of the material and nanosphere template size. This indicates that plasmon modes supported by voids of such thick layers must contribute to the high enhancement of the two-photon processes excited in the near IR. Furthermore, an increased roughness of the void rims, especially when void heights are above the template sphere equator (for example compare Figure 1C with Figure 1E) could add to the electromagnetic field enhancement and higher signals in SEHRS and SHG, in line with enhanced SHG from nanocavities with rough rims that has been reported previously.[26]

Of the samples prepared with the polystyrene template spheres of different sizes, the voids with 200 and 300 nm nanosphere templates showed significantly stronger SHG and SEHRS enhancement than the voids made with 600 nm templates (data not shown). Therefore, we fabricated nanovoid arrays with 200 and 300 nm nanosphere templates and uniform metal thickness in a conventional three-electrode electrochemical setup. In order to obtain the desired void diameter and height according to the values in Table 1, a thorough optimization procedure using a high-throughput scanning droplet cell

(SDC),[27] was carried out, described in detail in the Supporting Information. Multiple spots (1 mm in diameter, see Figure S3 in the Supporting Information) were fabricated. **Figure 3** shows representative scanning electron micrographs of the samples produced with different templates, termed Ag(200), Ag(300), Au(200), and Au(300), together with the void opening sizes determined by SEM to verify the matching with the sizes that gave highest two-photon signals in the gradient substrates.

The optimized nanovoid samples were used for SEHRS and SHG experiments, both excited at 1064 nm with picosecond laser pulses. **Figure 4**A shows the quadratic dependence of the SHG signal on excitation intensity for Ag(200) and Au(200) nanovoids. This confirms the two-photon parametric process of SHG. Likewise, the square dependence of the SEHRS signal on laser excitation intensity is displayed in Figure 4B. The SHG and SEHRS signals generated by the silver nanovoids are stronger than those from the gold voids. While with silver nanovoids, SHG and SEHRS could be observed already at excitation intensities from ≈10^8 Wcm^{-2}, with gold voids a peak laser intensity above ≈10^9 Wcm^{-2} is required. The square dependence of the two-photon signals indicates a high stability of the plasmonic structures over the applied intensity range. However, the gold voids are more stable than the silver voids at higher laser intensities. For the gold voids, the square dependence of both SHG and SEHRS is maintained for peak laser intensities of up to 2×10^{10} Wcm^{-2} (Figure 4A,B), while for silver voids the signal dependence on excitation intensity above 2×10^9 Wcm^{-2} shows a more linear rather than quadratic character (data not shown here). The observation of a strong and stable SEHRS signal generated by the gold nanovoids is very promising for several applications and supports the so far very few reports of SEHRS with gold nanostructures.[4a,13,28]
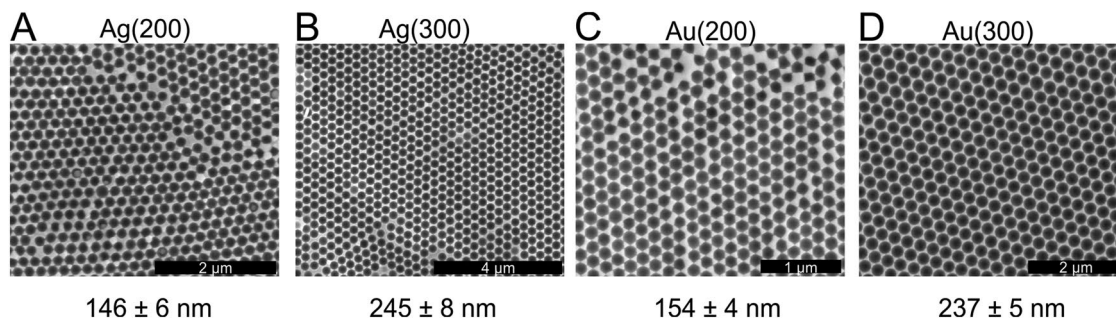

A Ag(200)	B Ag(300)	C Au(200)	D Au(300)
146 ± 6 nm	245 ± 8 nm	154 ± 4 nm	237 ± 5 nm

Figure 3. Scanning electron micrographs of the A,B) silver and C,D) gold nanovoids with A,C) 200 nm and B,D) 300 nm polymer nanosphere templates obtained after optimization using scanning droplet cell (SDC) electrodeposition. Below the SEM images the average sizes of the void openings are listed, in all cases the metal film is above the equator of the spheres.
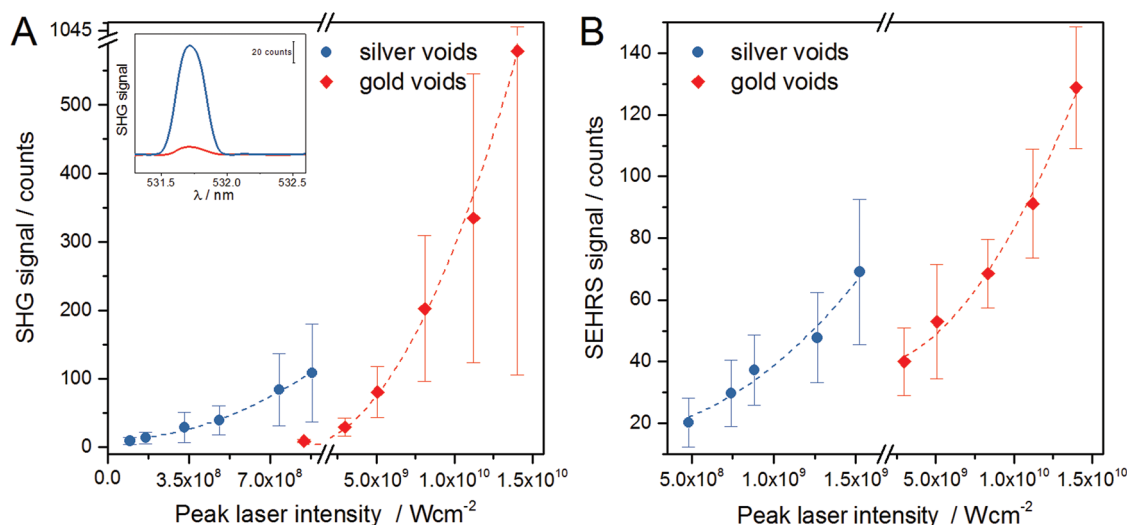
Figure 4. A) SHG signal, and B) SEHRS signal of the crystal violet band at 1585 cm^{-1} from Au(200) and Ag(200) nanovoids as a function of the applied peak laser intensity. The dotted lines are the fitted quadratic curves ($ax^2 + b$) to the data points. The inset in (A) shows the SHG signal from gold and silver voids at 9×10^8 Wcm^{-2}. Excitation: 1064 nm; acquisition time: 1 s (A) and 60 s (B).

As can be inferred from SHG imaging data on both kinds of silver and gold nanovoids (**Figure 5**), the SHG signal variation within larger microscopic areas within one substrate and for the same metal voids with different diameters is quite similar (compare Figure 5A with Figure 5B and Figure 5C with Figure 5D). According to the two-photon focal spot diameter, in our experiments estimated to be ≈415 nm, the SHG signal at 1064 nm excitation originates from less than two nanovoids at each pixel of an SHG image. Therefore, the signal can vary, depending on which part of the nanostructure is responsible for the observed SHG, in addition to small inhomogeneities due to the metal film growth. Despite the small variation between the different positions in one respective substrate, when comparing the different panels in Figure 5, the Ag(200) voids display the strongest SHG signals (Figure 5A), followed by the Ag(300) (Figure 5B), and Au(200) nanovoids (Figure 5C). The weakest overall SHG was observed with the Au(300) samples (Figure 5D). The same sequence of relative SHG signal strength was observed also in experiments carried out at 850 nm excitation (data not shown).

SEHRS spectra of crystal violet were obtained with gold and silver nanovoids with 200 and 300 nm nanosphere templates by scanning areas of the nanovoid substrates. Representative spectra for the four different nanovoid structures are presented in **Figure 6**, and SEHRS maps of the scanned areas based on the crystal violet ring stretching vibration at 1585 cm^{-1} are shown in **Figure 7**. The spectra resemble those previously reported using gold and silver nanoparticles.[4a,13,29] Ag(200) voids show the highest and Au(300) the lowest SEHRS enhancement (Figure 7). However, different from the comparison of SHG signals, in SEHRS Au(200) voids give higher signals than Ag(300) nanovoids (compare Figure 7B with Figure 7C). As evidenced by the signal being on the same order of magnitude for SEHRS spectra obtained from different macroscopic nanovoid spots, the enhancement provided by Ag(300), Au(200), and Au(300) nanostructures, respectively, is very homogeneous (compare different maps within Figure 7B–D). Since SEHRS is an extremely sensitive probe of both plasmonic properties[13] and surface potential,[8b] the homogeneous enhancement supports the SEM and chronoamperometry data (see Figure S3 in the Supporting
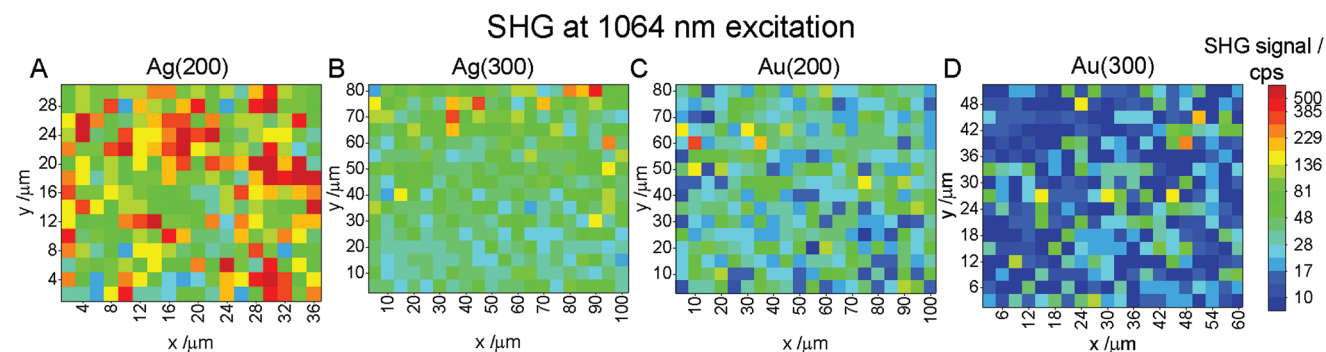
SHG at 1064 nm excitation

Figure 5. Images based on the SHG signal at 532 nm from A,B) silver and C,D) gold nanovoids produced with A,C) 200 nm and B,D) 300 nm nanosphere templates corresponding to void opening sizes of A) ≈146 nm, B) ≈245 nm, C) ≈154 nm, and D) ≈237 nm. Excitation: 1064 nm; acquisition time: 1 s, peak laser intensity: 7×10^8 Wcm^{-2} (3 mW average power); step size: 2 µm (A), 5 µm (B,C), and 3 µm (D).

**ADVANCED
SCIENCE NEWS**

www.advancedsciencenews.com

**ADVANCED
OPTICAL
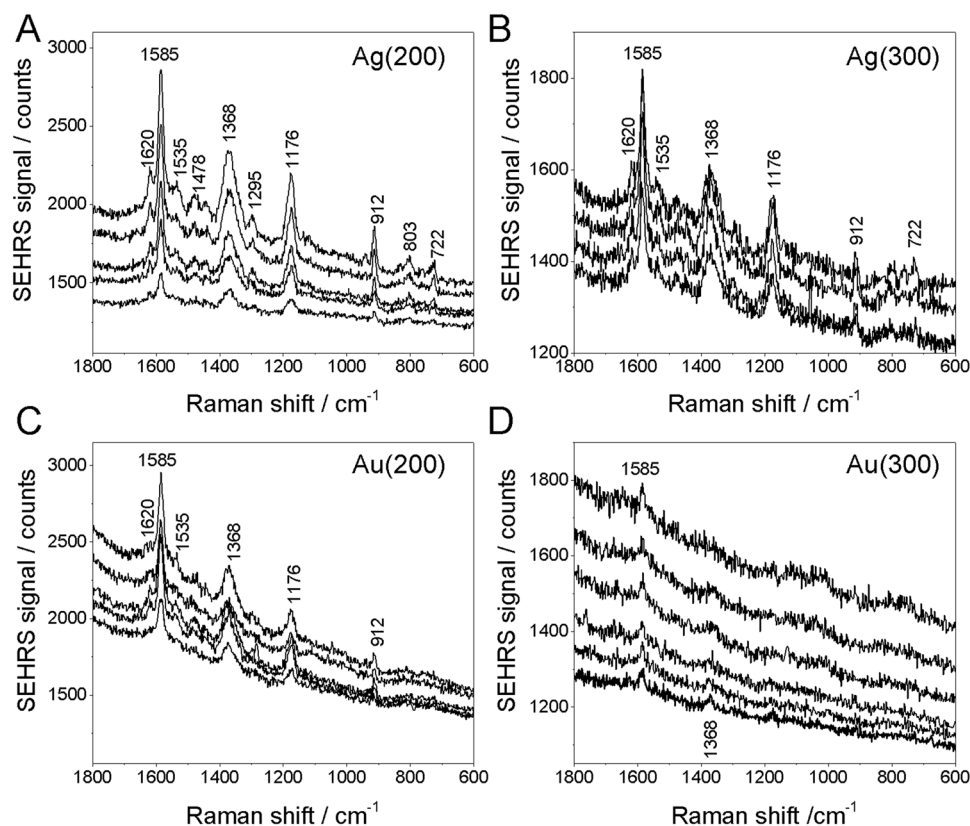MATERIALS**

www.advopticalmat.de

Figure 6. Representative SEHRS spectra of crystal violet obtained from a solution placed as droplet onto the nanovoid substrate, extracted from the SEHRS maps shown in Figure 7 obtained with A,B) silver and C,D) gold nanovoids produced with A,C) 200 nm and B,D) 300 nm nanosphere templates corresponding to void opening sizes of A) ≈146 nm, B) ≈245 nm, C) ≈154 nm, and D) ≈237 nm. Excitation: 1064 nm; acquisition time: 60 s, laser peak intensity: 1×10^{10} Wcm^{-2} (50 mW average power); concentration of crystal violet: 10^{-5} M.

Information) regarding the extremely reproducible fabrication of the different macroscopic nanovoid spots on one silicon wafer by means of SDC. Although the Ag(200) voids showed

more significant variation of the SEHRS intensities between different spots with nanovoid structures (compare different maps in Figure 7A), the homogeneous SEHRS signals within each
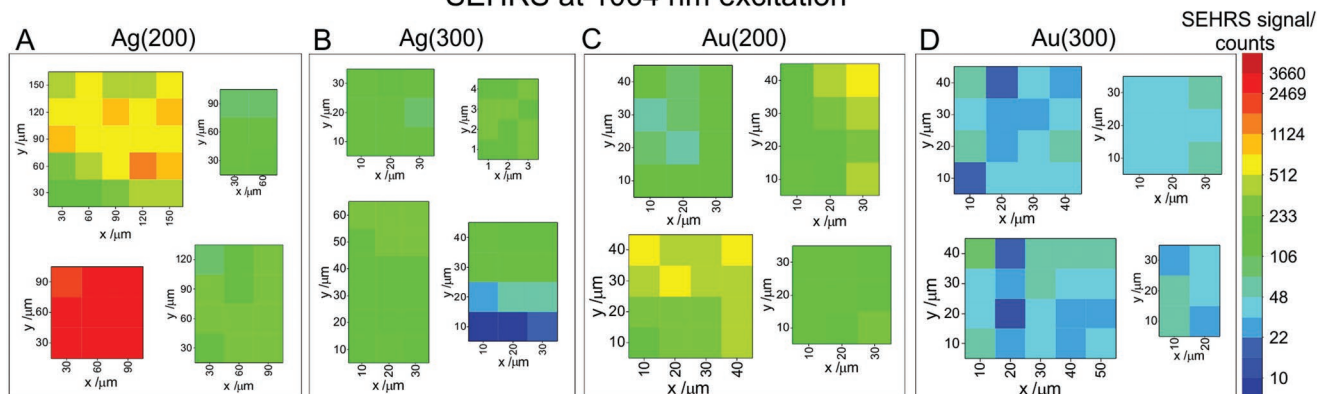

Figure 7. SEHRS maps of A,B) silver and C,D) gold nanovoids produced with A,C) 200 nm and B,D) 300 nm nanosphere templates, corresponding to void opening sizes of A) ≈146 nm, B) ≈245 nm, C) ≈154 nm, and D) ≈237 nm, based on the intensity of the crystal violet band at 1585 cm^{-1}. Each map was obtained from a different macroscopic spot. Excitation: 1064 nm; acquisition time: 60 s, laser peak intensity: 1×10^{10} Wcm^{-2} (50 mW average power); concentration of crystal violet in a droplet placed on the surface of the nanovoid arrays: 10^{-5} M; step size: 30 μm (A), 10 μm (B–D), and 1 μm for the right uppermost map in (B).

ADVANCED
SCIENCE NEWS
www.advancedsciencenews.com

ADVANCED
OPTICAL
MATERIALS
www.advopticalmat.de

respective spot indicate a high homogeneity at the microscopic level.

By comparing the SEHRS spectra with a normal HRS spectrum of crystal violet, we estimate enhancement factors for the nanovoids between 10^3 and 10^4 for Au(200) and Ag(200) and $\approx 10^3$ for Au(300) and Ag(300). Our assessments are very conservative because we assume that all crystal violet molecules in the two-photon focal volume take part in the SEHRS process, although not all molecules will be at the nanovoid surface, and even the estimated maximum possible coverage of the nanovoid surface with crystal violet molecules must be less than 1% at the chosen crystal violet concentration. For comparison, in previous work we estimated enhancement factors for aggregates of gold and silver nanoparticles in solution to be on the order of 10^6–10^7.[13] In spite of the lower SEHRS signals obtained with the nanovoid arrays here, the latter present numerous advantages for SEHRS experiments due to the more homogeneous and reproducible enhancement, as well as the high stability of the substrate structure, which cannot be modified by chemical or electrostatic interactions with the analyte molecules as found for nanoaggregates in solution.[13]

High stability and reproducibility also become obvious in an experiment where SEHRS spectra and SHG from Ag(200) nanovoids with crystal violet solution were collected in the same position in subsequent raster scans. **Figure 8** shows the SHG signal, SEHRS intensity and background in the respective SEHRS spectra at the particular measurement points. The intensity of the crystal violet vibrational bands clearly correlates with the observed background in the SEHRS spectra—the higher the SEHRS signal, the more pronounced are the background contributions (compare Figure 8B with Figure 8C). Possible origins of the background have been discussed in terms of the nanostructure properties for experiments with nanoaggregates previously.[10c,30] Moreover, at the sample positions where the SEHRS intensity is high, strong SHG is observed (compare Figure 8A with Figure 8B). Together with the observation that the highest SHG and SEHRS data are obtained for nanovoids of the same sizes from gradient nanovoid substrates discussed above (Table 1), this indicates that those nanostructures supporting high SEHRS enhancement also provide high signals in SHG. Based on this observation, SHG can be used for fast screening of suitable SEHRS substrates, rather than utilizing optimized SERS nanomaterials for SEHRS experiments, which has often been the strategy for designing SEHRS substrates so far. Prescreening of a microscopic surface, e.g., of a sensor probed by SEHRS, by fast acquisition of the monochromatic SHG signal, can ensure selection of sample positions that provide optimum enhancement for the collection of two-photon vibrational spectra.

3. Conclusion

We have investigated nonlinear optical properties of gold and silver nanovoid arrays by means of SEHRS and SHG. We successfully employed bipolar electrodeposition utilizing nanosphere templates of three different sizes to fabricate a multitude of different gold and silver nanovoid structures with gradually changing thickness on a single sample surface, respectively, and identified those void structural parameters that provide high enhancement of SEHRS and SHG. SEHRS and SHG screening experiments along the gradient nanovoid samples revealed that nanovoids with different heights show significantly different enhancement in both two-photon processes. In particular, nanovoids yielding the strongest SEHRS at 1064 nm and SHG at 850 nm excitation have nearly the same structural parameters. This suggests that utilizing SHG as a fast screening tool for identifying nanostructures that support high SEHRS enhancement could provide more advantages than adapting substrates optimized for one-photon SERS in SEHRS experiments.
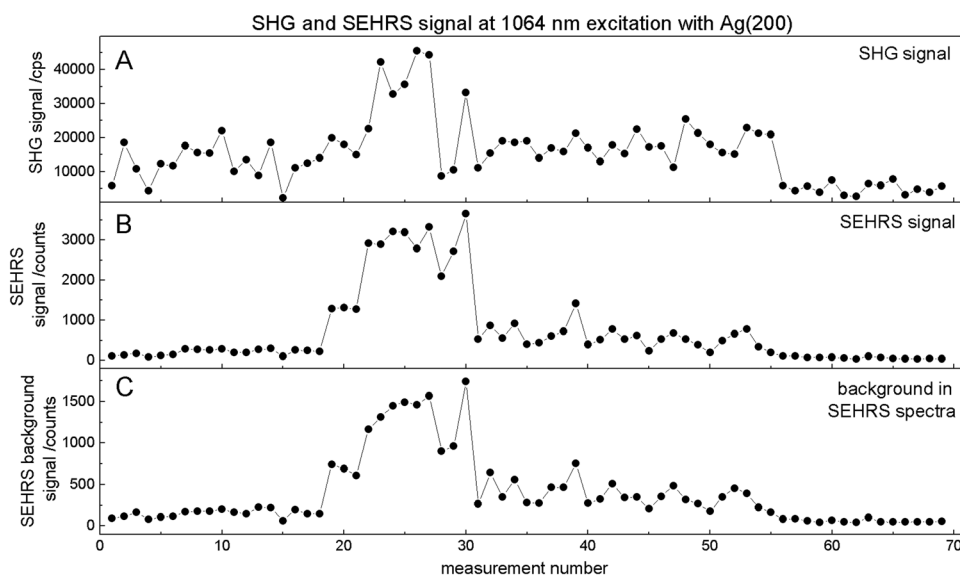

Figure 8. A) SHG signal, B) SEHRS signal of the crystal violet band at 1585 cm^{-1}, and C) background in the respective SEHRS spectra in (B) obtained from Ag(200) substrate with 10^{-5} M crystal violet solution. The data was obtained from four different macroscopic spots—measurement number 1–21 from spot 1, 22–30 from spot 2, 31–55 from spot 3, and 56–69 from spot 4.

**ADVANCED
SCIENCE NEWS**

www.advancedsciencenews.com

**ADVANCED
OPTICAL
MATERIALS**

www.advopticalmat.de

The optimum void sizes giving highest enhancement of the two-photon process of SEHRS at excitation with 1064 nm light differ from nanovoid sizes that were identified to provide highest enhancement of 532 nm one-photon excited SERS,[21a] pointing toward the importance of plasmon modes with resonances at near-IR frequencies. The observation that voids with a normalized thickness of ≈0.8 support the highest SEHRS and SHG signals, independent of the material or template size, suggests that near IR excitation wavelengths match the plasmon resonances that exist in such thick nanovoids. Furthermore, the data could indicate an enhancement of EM fields due to increased roughness of the nanovoid rims and metal film around them.

Comparing the potential of different nanovoid structures for SEHRS applications, both gold and silver voids with 200 and 300 nm nanosphere templates and void opening sizes of ≈150 and ≈240 nm, respectively, provide sufficient enhancement. Silver nanovoids yield stronger SEHRS enhancement than gold voids, but gold nanovoid arrays show improved stability at high laser excitation intensities. The estimated enhancement factors for gold and silver nanovoids are slightly lower than the enhancement by nanoparticle aggregates of the same materials in solution. Nevertheless, nanovoid substrates reveal many advantages for SEHRS spectroscopy and imaging applications with respect to homogeneity, reproducible fabrication, and stability that remained unaddressed so far in SEHRS experiments with other plasmonic substrates.

4. Experimental Section

Preparation of Nanovoid Gradient Substrates: Gradient gold and silver nanovoid substrates were prepared by bipolar electrodeposition as reported previously and described in detail in ref. [21] Briefly, Au/Ag-coated Si wafers (8 nm Ti adhesion layer, 150 nm Ag/Au coating) were decorated with polystyrene nanospheres (Thermo Fisher Scientific, USA) utilizing a Langmuir–Blodgett trough (KSV Instruments, FIN). 150 µL nanospheres were mixed with 300 µL EtOH and evenly distributed on the water surface. The film was compressed until a surface pressure of 50 mN m^{-1} was reached (using a 2 × 1 cm² Pt Wilhelmy plate). During vertical retraction (2 mm min^{-1}) the surface pressure was kept constant. Only samples offering a homogeneously covered surface confirmed by means of SEM were used for further experiments.

For the bipolar electrodeposition, an in-house built cell was used with a feeder electrode distance of d = 16 cm (carbon rods, Ø = 6 mm and 9 cm length, SGL Carbon, D).[21,31] Details on the principle of this deposition approach are provided in the Supporting Information. Prior to the electrodeposition, the electrodes were incubated in the plating solution for 10 min to ensure complete wetting of the surface. Bipolar electrodepositions were carried out while keeping the field gradient across the BE constant at 3 V for 60 s. For this purpose, the voltage difference between the feeder electrodes was varied between 6 and 10 V depending on the length of the BE. The depositions were done using commercial plating solutions (Ag: MetSil 500 CNF, 31 g L^{-1}, Au: ECF 60 gold plating solution 15 g L^{-1} mixed with E3 brightener EC4073 (v/v 200:1), Metalor Technologies, CH). After electrodeposition, the BEs were cleaned with EtOH and H$_2$O followed by incubation (60 min) in dichloromethane in order to dissolve the nanospheres.

Reproduction of Optimal Nanovoid Structures for Two-Photon Experiments in a Three-Electrode Setup: The void sizes offering the highest enhancement in the two-photon optical experiments were determined by SEM and then reproduced using an in-house built SDC.[27] Briefly, a measuring cell consisting of a polytetrafluoroethylene opening (Ø = 6 mm) with an integrated counter (CE, Pt wire) and reference electrode (RE, Ag/AgCl/3 M KCl) was fixed to a step motor based XYZ micropositioning stage (OWIS, D). The cell was connected to a PGU-100 bipotentiostat (IPS Jaissle, D) while the signal was read out utilizing an AD/DA converter. The experiments were carried by means of a software programmed using Microsoft Visual Basic 6.

Electrodeposition parameters such as time and potential in the conventional three-electrode setup were optimized systematically until the desired structures were obtained. In particular, as described in detail in the Supporting Information, the void opening sizes were analyzed as a function of the applied potential (Figure S4, Supporting Information). Furthermore, the approximate height of the resulting voids could be inferred from the shape of the chronoamperometric curve (Figures S5 S3, Supporting Information). The parameters used for SDC electrodeposition refinement as well as the final parameters are given in **Table 2**.

SEM Characterization: Scanning electron micrographs of nanovoid structures were taken using a Quanta 3D ESEM (FEI, USA) operating at 30 kV. The internal function of the instrument for measuring distances was used to image the gradient nanovoid substrates at the desired positions. The void diameters were determined by analyzing the SEM images with ImageJ V1.51.[32]

Second Harmonic Generation and Hyper Raman Experiments: To excite SHG and SEHRS, a laser operating at 1064 nm with 6 fs pulses at 75 MHz repetition rate was used. A drop of water or aqueous crystal violet solution (10^{-5} M) was placed on the nanovoid substrates, the excitation light was focused onto the samples through a 60× water immersion objective (NA 1.2), and the SHG and hyper Raman light, respectively, were detected in backscattering geometry by a single-stage spectrograph with a nitrogen cooled charge coupled device (CCD) detector. The spectral resolution was ≈3–6 cm^{-1} considering the full spectral range. The SEHRS spectra were frequency calibrated using a spectrum of a toluene/acetonitrile (1:1) mixture. The SHG signals were filtered with polarization-insensitive dichroic and bandpass filters with 20 nm full width. Alternatively, SHG was also excited at 850 nm using a laser operating with 150 fs pulses at 73 MHz repetition rate. The light was focused onto the nanovoid structures through a 10× microscope objective (NA 0.3), and the backscattered SHG light was filtered and detected as described above.

Supporting Information

Supporting Information is available from the Wiley Online Library or from the author.

Table 2. Experimental parameters during SDC electrodeposition refinement.

Substrate	Potential applied (vs Ag/AgCl/3 M KCl) [mV]	Increment [mV]	Final electrodeposition parameters (240 s) [mV]
Ag(200)	−650 to −800	10	−725
Ag(300)	−650 to −800	10	−695
Au(200)	−500 to −575	5	−540
Au(300)	−500 to −650	10	−545

Conflict of Interest

The authors declare no conflict of interest.

[1] a) W. R. Zipfel, R. M. Williams, W. W. Webb, *Nat. Biotechnol.* **2003**, *21*, 1369; b) F. Helmchen, W. Denk, *Nat. Methods* **2005**, *2*, 932.

[2] a) V. N. Denisov, B. N. Mavrin, V. B. Podobedov, *Phys. Rep.* **1987**, *151*, 1; b) L. D. Ziegler, *J. Raman Spectrosc.* **1990**, *21*, 769.

[3] a) R. Shimada, H. Kano, H.-O. Hamaguchi, *Opt. Lett.* **2006**, *31*, 320; b) A. Myers Kelley, *J. Phys. Chem. A* **2008**, *112*, 11975.

[4] a) J. Kneipp, H. Kneipp, K. Kneipp, *Proc. Natl. Acad. Sci. USA* **2006**, *103*, 17149; b) K. Kneipp, H. Kneipp, J. Kneipp, *Chem. Sci.* **2015**, *6*, 2721; c) F. Madzharova, Z. Heiner, J. Kneipp, *Chem. Soc. Rev.* **2017**, *46*, 3980.

[5] a) A. V. Baranov, Y. S. Bobovich, *JETP Lett.* **1982**, *36*, 339; b) D. V. Murphy, K. U. Vonraben, R. K. Chang, P. B. Dorain, *Chem. Phys. Lett.* **1982**, *85*, 43.

[6] a) M. Fleischmann, P. J. Hendra, A. J. McQuillan, *Chem. Phys. Lett.* **1974**, *26*, 163; b) M. G. Albrecht, J. A. Creighton, *J. Am. Chem. Soc.* **1977**, *99*, 5215; c) D. L. Jeanmaire, R. P. Van Duyne, *J. Electroanal. Chem. Interfacial Electrochem.* **1977**, *84*, 1.

[7] a) S. J. Cyvin, J. E. Rauch, J. C. Decius, *J. Chem. Phys.* **1965**, *43*, 4083; b) J. H. Christie, D. J. Lockwood, *J. Chem. Phys.* **1971**, *54*, 1141.

[8] a) J. T. Golab, J. R. Sprague, K. T. Carron, G. C. Schatz, R. P. V. Duyne, *J. Chem. Phys.* **1988**, *88*, 7942; b) J. C. Hulteen, M. A. Young, R. P. van Duyne, *Langmuir* **2006**, *22*, 10354; c) N. Valley, L. Jensen, J. Autschbach, G. C. Schatz, *J. Chem. Phys.* **2010**, *133*, 054103; d) F. Madzharova, Z. Heiner, J. Kneipp, *J. Phys. Chem. C* **2017**, *121*, 1235; e) H. K. Turley, Z. Hu, L. Jensen, J. P. Camden, *J. Phys. Chem. Lett.* **2017**, *8*, 1819.

[9] a) W. Leng, H. Y. Woo, D. Vak, G. C. Bazan, A. Myers Kelley, *J. Raman Spectrosc.* **2006**, *37*, 132; b) M. Gühlke, Z. Heiner, J. Kneipp, *J. Phys. Chem. C* **2016**, *120*, 20702; c) F. Madzharova, Z. Heiner, M. Gühlke, J. Kneipp, *J. Phys. Chem. C* **2016**, *120*, 15415; d) M. J. Trujillo, J. P. Camden, *ACS Omega* **2018**, *3*, 6660.

[10] a) J. Kneipp, H. Kneipp, B. Wittig, K. Kneipp, *Nano Lett.* **2007**, *7*, 2819; b) Y. Kitahama, H. Hayashi, T. Itoh, Y. Ozaki, *Analyst* **2017**, *142*, 3967; c) M. Guhlke, Z. Heiner, J. Kneipp, *Phys. Chem. Chem. Phys.* **2015**, *17*, 26093.

[11] a) M. Guhlke, Z. Heiner, J. Kneipp, *Phys. Chem. Chem. Phys.* **2016**, *18*, 14228; b) Z. Heiner, M. Guhlke, V. Zivanovic, F. Madzharova, J. Kneipp, *Nanoscale* **2017**, *9*, 8024.

[12] W.-H. Li, X.-Y. Li, N.-T. Yu, *Chem. Phys. Lett.* **1999**, *305*, 303.

[13] F. Madzharova, Z. Heiner, J. Simke, S. Selve, J. Kneipp, *J. Phys. Chem. C* **2018**, *122*, 2931.

[14] a) A. Shiohara, Y. Wang, L. M. Liz-Marzán, *J. Photochem. Photobiol., C* **2014**, *21*, 2; b) N. Guillot, M. L. de la Chapelle, *J. Nanophotonics*

[15] K. Ikeda, M. Takase, Y. Sawai, H. Nabika, K. Murakoshi, K. Uosaki, *J. Chem. Phys.* **2007**, *127*, 111103.

[16] a) S. Zhu, C. Fan, P. Ding, E. Liang, H. Hou, Y. Wu, *Sci. Rep.* **2018**, *8*, 11891; b) J. Butet, O. J. F. Martin, *J. Phys. Chem. C* **2015**, *119*, 15547.

[17] a) C. K. Chen, A. R. B. de Castro, Y. R. Shen, *Phys. Rev. Lett.* **1981**, *46*, 145; b) M. Moskovits, *Rev. Mod. Phys.* **1985**, *57*, 783; c) B. Metzger, L. Gui, J. Fuchs, D. Floess, M. Hentschel, H. Giessen, *Nano Lett.* **2015**, *15*, 3917; d) N. Subramaniyam, A. Shah, C. Dreser, A. Isomäki, M. Fleischer, M. Sopanen, *Appl. Phys. Lett.* **2018**, *112*, 233109.

[18] a) T. A. Kelf, Y. Sugawara, R. M. Cole, J. J. Baumberg, M. E. Abdelsalam, S. Cintra, S. Mahajan, A. E. Russell, P. N. Bartlett, *Phys. Rev. B* **2006**, *74*, 245415; b) R. M. Cole, J. J. Baumberg, F. J. Garcia de Abajo, S. Mahajan, M. Abdelsalam, P. N. Bartlett, *Nano Lett.* **2007**, *7*, 2094; c) S. Chen, L. Meng, J. Hu, Z. Yang, *Plasmonics* **2015**, *10*, 71.

[19] a) S. Cintra, M. E. Abdelsalam, P. N. Bartlett, J. J. Baumberg, T. A. Kelf, Y. Sugawara, A. E. Russell, *Faraday Discuss.* **2006**, *132*, 191; b) X. Lang, T. Qiu, Y. Yin, F. Kong, L. Si, Q. Hao, P. K. Chu, *Langmuir* **2012**, *28*, 8799; c) N. G. Tognalli, A. Fainstein, E. J. Calvo, M. Abdelsalam, P. N. Bartlett, *J. Phys. Chem. C* **2012**, *116*, 3414; d) M. Kahraman, P. Daggumati, O. Kurtulus, E. Seker, S. Wachsmann-Hogiu, *Sci. Rep.* **2013**, *3*, 3396; e) X. Zhu, L. Shi, M. S. Schmidt, A. Boisen, O. Hansen, S. Zi, S. Xiao, N. A. Mortensen, *Nano Lett.* **2013**, *13*, 4690.

[20] A. Kuchmizhak, O. Vitrik, Y. Kulchin, D. Storozhenko, A. Mayor, A. Mirochnik, S. Makarov, V. Milichko, S. Kudryashov, V. Zhakhovsky, N. Inogamov, *Nanoscale* **2016**, *8*, 12352.

[21] a) D. Öhl, Y. U. Kayran, J. R. C. Junqueira, V. Eßmann, T. Bobrowski, W. Schuhmann, *Langmuir* **2018**, *34*, 12293; b) Y. U. Kayran, V. Eßmann, S. Grützke, W. Schuhmann, *ChemElectroChem* **2016**, *3*, 399.

[22] a) M. I. Stockman, D. J. Bergman, C. Anceau, S. Brasselet, J. Zyss, *Phys. Rev. Lett.* **2004**, *92*, 057402; b) S. I. Bozhevolnyi, J. Beermann, V. Coello, *Phys. Rev. Lett.* **2003**, *90*, 197403; c) C. Anceau, S. Brasselet, J. Zyss, P. Gadenne, *Opt. Lett.* **2003**, *28*, 713.

[23] M. Schmidt, N. G. Tognalli, M. A. Otte, M. I. Alonso, B. Sepúlveda, A. Fainstein, A. R. Goñi, *Plasmonics* **2013**, *8*, 921.

[24] S. Mahajan, M. Abdelsalam, Y. Suguwara, S. Cintra, A. Russell, J. Baumberg, P. Bartlett, *Phys. Chem. Chem. Phys.* **2007**, *9*, 104.

[25] S. Mahajan, R. M. Cole, B. F. Soares, S. H. Pelfrey, A. E. Russell, J. J. Baumberg, P. N. Bartlett, *J. Phys. Chem. C* **2009**, *113*, 9284.

[26] A. Salomon, M. Zielinski, R. Kolkowski, J. Zyss, Y. Prior, *J. Phys. Chem. C* **2013**, *117*, 22377.

[27] a) K. Sliozberg, D. Schäfer, T. Erichsen, R. Meyer, C. Khare, A. Ludwig, W. Schuhmann, *ChemSusChem* **2015**, *8*, 1270; b) R. Meyer, K. Sliozberg, C. Khare, W. Schuhmann, A. Ludwig, *ChemSusChem* **2015**, *8*, 1279.

[28] a) L. A. Lipscomb, S. Nie, S. Feng, N.-T. Yu, *Chem. Phys. Lett.* **1990**, *170*, 457; b) V. Živanović, F. Madzharova, Z. Heiner, C. Arenz, J. Kneipp, *J. Phys. Chem. C* **2017**, *121*, 22958.

[29] a) W. Leng, A. M. Kelley, *J. Am. Chem. Soc.* **2006**, *128*, 3492; b) T. Itoh, Y. Ozaki, H. Yoshikawa, T. Ihama, H. Masuhara, *Appl. Phys. Lett.* **2006**, *88*, 084102.

[30] a) T. Itoh, H. Yoshikawa, K.-I. Yoshida, V. Biju, M. Ishikawa, *J. Chem. Phys.* **2010**, *133*, 124704; b) G. Brehm, G. Sauer, N. Fritz, S. Schneider, S. Zaitsev, *J. Mol. Struct.* **2005**, *735–736*, 85.

[31] V. Eßmann, D. Jambrec, A. Kuhn, W. Schuhmann, *Electrochem. Commun.* **2015**, *50*, 77.

[32] C. A. Schneider, W. S. Rasband, K. W. Eliceiri, *Nat. Methods* **2012**, *9*, 671.